Mater Renew Sustain Energy (2016) 5:3
DOI 10.1007/s40243-016-0067-z

ORIGINAL PAPER

Improving the cycling stability of $Na_3V_2(PO_4)_3$ nanoparticle in aqueous sodium ion batteries by introducing carbon support

Huajun Zhou[1] · Z. Ryan Tian[1,2] · Simon S. Ang[1,3]

Received: 29 July 2015 / Accepted: 21 January 2016 / Published online: 8 February 2016

Abstract Here we report the electrochemical performances of a $Na_3V_2(PO_4)_3$/C nanocomposite as a cathode material for aqueous sodium-ion batteries (SIBs). Compared to a previously reported $Na_3V_2(PO_4)_3$ microparticle, this nanocomposite demonstrated much improved cycling stability. While the improvement mainly attributed to the right pH and the carbon matrixmediated protection against the electrolyte, the capacity fade was mainly due to the deterioration of crystallinity and structure of the nanocomposite caused by various interactions between the nanocomposite and electrolyte. This work not only help to understand the degradation of $Na_3V_2(PO_4)_3$ in aqueous SIBs, but also shed light on the design and fabrication of electrode materials with high cycling stability for aqueous SIBs.

Keywords Sodium ion batteries · $Na_3V_2(PO_4)_3$ · Cathode · Aqueous batteries · Carbon coating

Introduction

Currently widely used lithium-ion batteries (LIBs) employ flammable and toxic organic solvents and expensive lithium-containing compounds, and thus present two major issues of safety and cost and find limits in large-scale applications. To address these issues and meet the vast need for energy storage, recently aqueous sodium-ion batteries (SIBs) with their capacities comparable to those of LIBs have received considerable interests [1–5]. On one hand, aqueous systems are safer as they could be neither flammable nor toxic; on the other hand, sodium is much less expensive than lithium due to its much more abundant natural reserve. Furthermore, the high ionic conductivity [2] of aqueous electrolytes can support fast charge–discharge processes.

Among electrode materials candidates for aqueous SIBs, sodium vanadium phosphates with sodium (Na) super ion conductor (NASICON) structures such as $NaVPO_4F$ [6], $Na_3V_2O(PO_4)_2F$ [7], and $Na_3VTi(PO_4)_3$ [8] have been widely investigated as cathodes for the following reasons. First, this structure features a highly covalent three-dimensional (3D) framework in which Na-ions can facilely diffuse in and out [9]; second, the strong covalent bonds can provide structural stability and safety. Though extensive studies have been investigated on the use of $Na_3V_2(PO_4)_3$ as electrode materials in non-aqueous SIBs [10–15], the use of $Na_3V_2(PO_4)_3$ as electrode materials in aqueous SIBs was first studied by Ji and Banks only very recently [16]. In that work, $Na_3V_2(PO_4)_3$ microparticle was tested as the cathode material, and its capacities were found to decay in a rather significant fashion (ca. 31 % capacity retention for the 30th cycle). The mechanism responsible for the capacity fade was not investigated either.

Here we report the use of $Na_3V_2(PO_4)_3$/C nanocomposite composed of $Na_3V_2(PO_4)_3$ nanoparticles and a carbon matrix as the cathode material for aqueous SIBs. The $Na_3V_2(PO_4)_3$ nanoparticle provides shorter Na-ion diffusion lengths than its micro-sized counterpart does while the carbon support could enhance the electrical conductivity of the electrode [10] and slow down its dissolution [1].

✉ Huajun Zhou
hxz001@uark.edu

[1] High Density Electronics Center, University of Arkansas, Fayetteville, AR 72701, USA

[2] Department of Chemistry and Biochemistry, University of Arkansas, Fayetteville, AR 72701, USA

[3] Department of Electrical Engineering, University of Arkansas, Fayetteville, AR 72701, USA

Compared to the previously reported $Na_3V_2(PO_4)_3$ microparticle, this nanocomposite indeed demonstrates much improved cycling stability. The mechanism responsible for the capacity fade was also investigated here.

Experimental methods

Syntheses of $Na_3V_2(PO_4)_3$/C nanocomposite

The nanocomposite was prepared by modifying a published procedure [10]. To a round-bottom flask containing 30 mL tetraethylene glycol (TEG) was added 0.246 g/3 mmol sodium acetate ($NaCH_3COO$), 0.697 g/2 mmol vanadium (III) acetylacetonate ($VO(C_5H_7O_2)_2$), and 0.345 g/3 mmol ammonium dihydrogen phosphate ($NH_4H_2PO_4$). The mixture was then stirred overnight at room temperature to afford a homogenous green solution, and the resultant solution was then heated at 320 °C for 72 h. The precipitate was collected by centrifugation, washed by ethanol and acetone each for 3 times respectively, and dried in a vacuum oven at 80 °C for 2 h. Then the resultant light-brown powders were annealed at 650 °C under Ar/H_2 (40/2 sccm) for 6 h and then at 800 °C under Ar flow (40 sccm) for 6 h to afford black powders.

Materials characterizations

The phase purity was characterized by a Rigaku MiniFlex II Desktop X-ray diffractometer using monochromatized Cu-Kα radiation ($\lambda = 1.5418$ Å) at 30 kV and 15 mA. A continuous scan mode was used to collect the diffraction data from 10 to 60° at a speed of 0.2°/min. The morphologies were investigated by an FEI Nova NanoSEM scanning electron microscope (SEM) equipped with a field emission gun operated at 10 kV and by an FEI Titan 80–300 transmission electron microscope (TEM). To minimize charging problems, samples for SEM were coated with thin Au layers. Raman spectra were recorded on a homemade μRaman spectroscope that was composed of a 632.8 nm He–Ne excitation laser, an iHR 550 HORIBA spectrometer, and a Si CCD detector. Prior to Raman the measurement, the system was calibrated using a bulk Si. Elemental analysis was done in Atlantic Microlab Inc. to determine the weight percentage (~20wt %) of carbon species in the $Na_3V_2(PO_4)_3$/C nanocomposite. ICP-MS analysis revealed the mole ratio of Na:V:P to be 3.00:2.00:3.00, further suggesting the pure phase of $Na_3V_2(PO_4)_3$/C.

Electrochemical measurements

A three-electrode beaker-type cell was used to test the electrochemical performances of $Na_3V_2(PO_4)_3$/C nanocomposite in an aqueous system. A large piece of pure platinum, a Ag/AgCl/1 M KCl electrode (0.235 V vs. NHE), and 1 M Na_2SO_4 aqueous solution served as the counter electrode, reference electrode, and electrolyte, respectively. The working electrode was prepared by mixing the nanocomposite, super P carbon black, and polytetrafluoroethylene (PTFE) in a weight ratio of 75:20:5 onto a stainless steel foil of ~0.3 cm^2 area. The electrodes were dried in a vacuum oven at 80 °C overnight, and then pressed at a pressure of 20 MPa using a PHI manual compression presses. The loading of each electrode was controlled to be 1–2 mg cm^{-2}, and the thickness was ~50 μm. Before the cell assembly, the electrolyte was bubbled with Ar for 60 min while the platinum foil was first rinsed in acetone and then repeatedly ultrasonicated in deionized water. Cells were assembled in an Ar atmosphere. Cyclic voltammetry (CV) was performed on a Solartron SI 1287 Electrochemical Interface at a scan rate of 0.5 mV s^{-1} from 0 to 0.8 V (vs. the reference electrode) while galvanostatic tests were performed on a BT 2000 battery tester. The electrochemical performances of this nanocomposite in a non-aqueous system were also tested as a reference. The electrode fabrication was the same as above except that here Al foil was used and electrodes were ~8 mm in diameter. The loading and thickness of each electrode was 1–2 mg cm^{-2} and ~50 μm, respectively. 2032-type coin cells were assembled in an MBraun glove box ($O_2 < 0.1$ ppm, $H_2O < 2$ ppm) while a Celgard 3501 microporous membrane was used as the separator. CV was performed on a Solartron SI 1287 electrochemical interface at a scan rate of 0.05 mV/s while galvanostatic tests were performed on a BT 2000 battery tester. 1 M $NaClO_4$ in EC/DMC (w/w = 1:2) and Na foil were used as the electrolyte and counter electrode.

Results and discussion

In the crystal structure of $Na_3V_2(PO_4)_3$, each VO_6 octahedron is connected to three PO4 tetrahedrons via corners to afford $[V_2(PO_4)_3]^{3-}$ ribbons along the *c* axis, and these ribbons are connected to each other through PO_4 tetrahedrons along the *a* axis to afford an open 3D framework where two kinds of Na ions reside (Fig. 1a). Na1 atoms reside between two adjacent $[V_2(PO_4)_3]^{3-}$ units within the same ribbons while Na2 atoms reside between adjacent ribbons. The channels along the *a* axis (Fig. 1a) and the *b* axis are the same in dimension, and are favored routes for Na-ion diffusion while the channel along the *a* axis is more favored [17]. The PLATON program [18] suggests that neither the pristine $Na_3V_2(PO_4)_3$ nor the anionic framework $[V_2(PO_4)_3]^{3-}$ can support physical adsorption of water. As confirmed by the space-filling model of the anionic

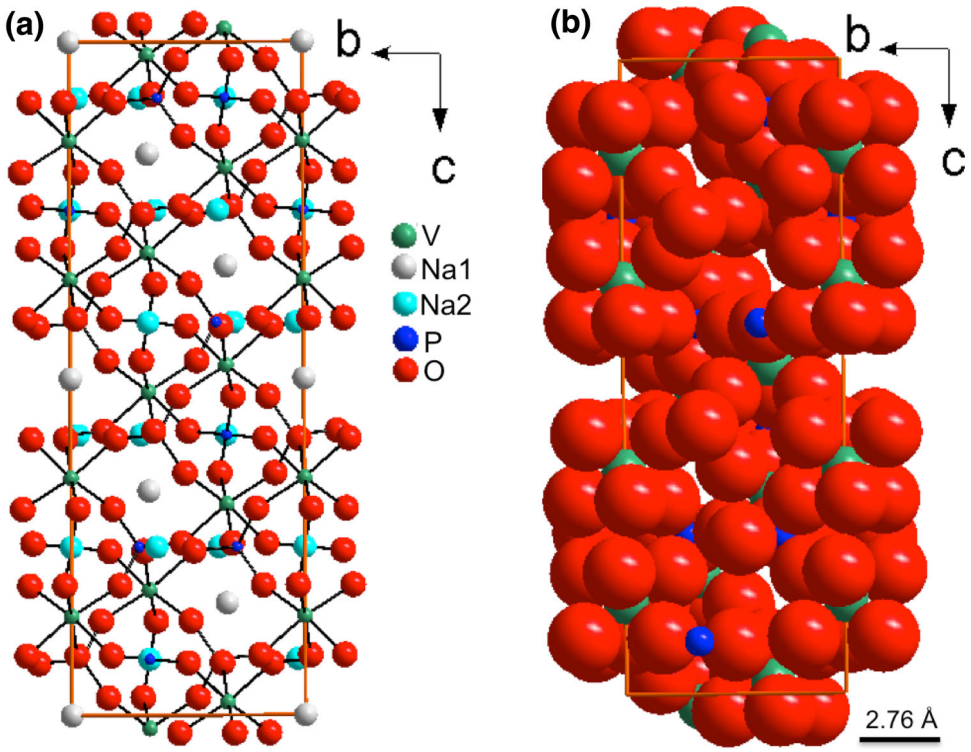

Fig. 1 **a** *Ball stick* model of a unit cell structure of $Na_3V_2(PO_4)_3$ viewed along the *a* axis; *orange lines* represent cell edges; **b** space-filling model of the anionic framework $[V_2(PO_4)_3]^{3-}$ in which Na-ions reside, indicating the channels are too small for physical adsorption of water molecules; the *scale bar* represents the diameter of a water molecule

framework (Fig. 1b, the radii of all atoms were assigned according to Shannon's work [19]), the cross section of the channel along the *a* axis in the anionic framework is $\sim 2.60 \times 0.12$ Å in dimension, making physical adsorption water (~ 2.76 Å in diameter) through the channels impossible. During the repeated charge–discharge cycles, $Na_3V_2(PO_4)_3$ is the Na-inserted phase while $NaV_2(PO_4)_3$ is the Na-extracted phase [12]. Compared to $Na_3V_2(PO_4)_3$, $NaV_2(PO_4)_3$ maintains the same structure but decreased lattice sizes (~ 8.3 % volume decrease) [12]. Therefore water adsorption cannot interfere with the Na-ion extraction-insertion during cycling. $Na_3V_2(PO_4)_3$ is different from some frameworks such as spinel-type lithium manganese oxide that can support simultaneous insertion-extraction of water and metal ions during cycling [20].

The powder X-ray diffraction (PXRD) pattern of the $Na_3V_2(PO_4)_3$/C nanocomposite obtained after annealing at 800 °C confirmed the NASICON structure with the R-3c space group (Fig. 2a) [9]. The SEM image in Fig. 2b indicates that $Na_3V_2(PO_4)_3$ nanoparticles were aggregated with their grain sizes being in the range of 60–120 nm. TEM analysis confirmed the presence of the carbon support (Fig. 2c). Raman spectrum in Fig. 2d clearly shows two distinct peaks, the D-band associated with sp3-hybridized carbon at ~ 1338 cm^{-1} and the G-band associated with sp2-hybridized carbon at ~ 1589 cm^{-1}. The intensity ratio of the D- and G-bands (ID/IG) is 1.10, indicating there are large amount of sp^2-carbon capable of providing high electronic conductivity. The lower intensity of G-band could be due to the interaction between the $Na_3V_2(PO_4)_3$ nanoparticles and carbon [1]. During the synthesis, tetraethylene glycol (TEG) molecules played a dual role: First, they provided a reducing environment [21] to stabilize V(III) in the presence of oxygen; Second, they functioned as a capping agent [10] on the as-synthesized $Na_3V_2(PO_4)_3$ nanoparticles and were then be converted to carbon species upon annealing.

The electrochemical performances of this nanocomposite were first investigated in non-aqueous electrolyte (Fig. 3) as a reference. Figure 3a shows the cyclic voltammograms (CVs) in the voltage range of 2.3–3.9 V vs. Na^+/Na at the scan rate of 0.05 mV/s. During the first scan, a pair of sharp peaks is observed: the oxidation (Na-ion extraction) and reduction peak (Na-ion insertion) are at 3.48 and 3.28 V. The average voltage (3.38 V) is close to the equilibrium voltage of V^{4+}/V^{3+} redox couple of this compound [11]. In subsequent up to ten scans, the peak positions also remain unchanged while the currents just decreased slightly, indicating the good reversibility for Na-ion extraction and insertion and the stability of the structure. Figure 3b shows the charge–discharge profiles at a current of 1 C in the range of 2.3–3.9 V (note that 1 C means the full capacity can be charged or discharged in 1 h and here 1 C $\approx$ 110 mA/g since the theoretical discharge capacity of $Na_3V_2(PO_4)_3$ is c.a. 110 mAh/g). An evident voltage plateau around 3.4 V was observed for both charge

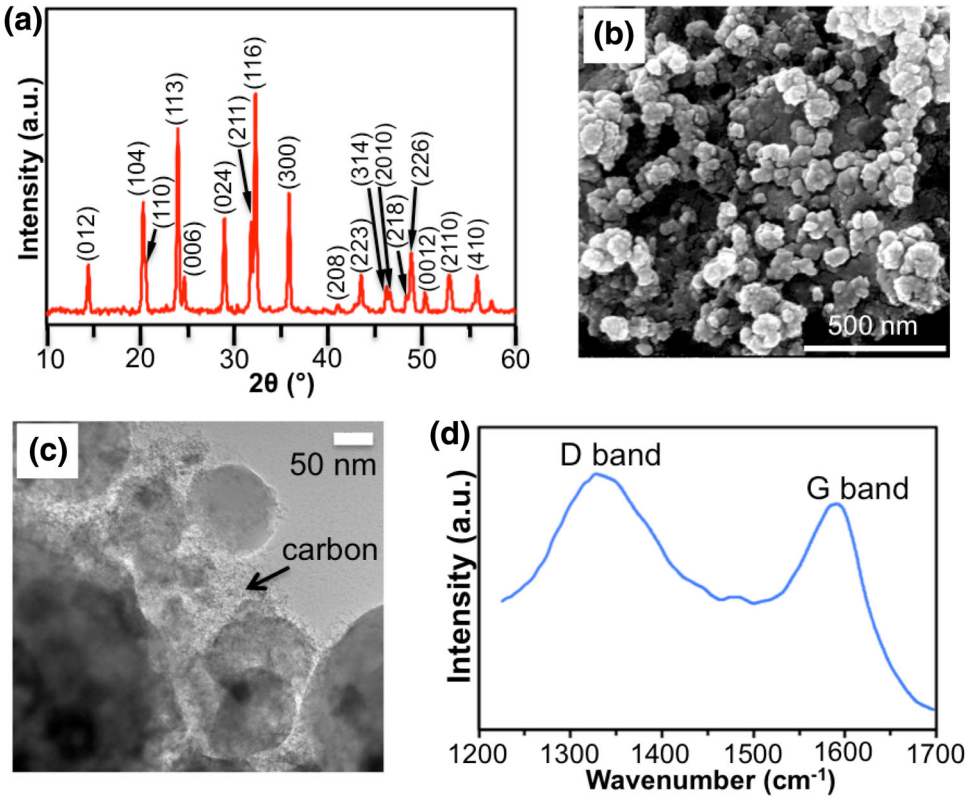

Fig. 2 Structural characterizations of the $Na_3V_2(PO_4)_3$/C nanocomposite. **a** Powder XRD pattern confirming the composition of $Na_3V_2(PO_4)_3$; **b** SEM image indicating the sizes; **c** TEM image indicating $Na_3V_2(PO_4)_3$ nanoparticles are embedded into a carbon matrix; **d** Raman spectrum indicating the characteristic of carbon species

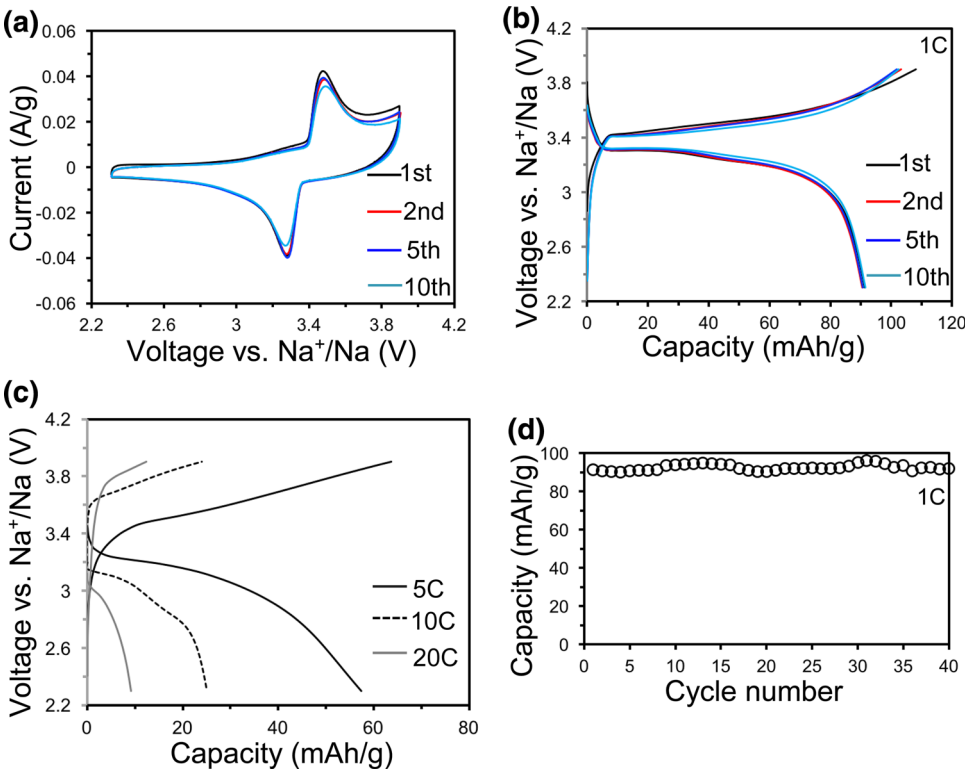

Fig. 3 Electrochemical performances of this $Na_3V_2(PO_4)_3$/C nanocomposite using 1 M $NaClO_4$ in EC/DMC (w/w = 1:2) as the non-aqueous electrolyte. **a** Cyclic voltammograms at the scan rate of 0.05 mV/s up to ten cycles. **b** Galvanostatic charge–discharge cycling profiles at 1 C. **c** Initial charge–discharge cycling profiles at 5 C, 10 C, and 20 C. **d** Discharge capacity evolution for 40 cycles at 1 C currents

and discharge, and the average polarization (i.e. the voltage difference between charge and discharge plateaus) is about 0.25 V. The $Na_3V_2(PO_4)_3$ in this nanocomposite delivers the initial charge capacity of 108.0 mAh/g and discharge capacity of 91.3 mAh/g (Note that the mass was based on that of $Na_3V_2(PO_4)_3$ while the carbon species constituted

∼wt 20 % of the nanocomposite). In comparison, different carbon species have been proven to significantly affect the initial discharge capacities of $Na_3V_2(PO_4)_3$/C composites which range from ∼30 mAh/g [11], to ∼70 mAh/g [22], and to 104 mAh/g [10]. The discharge capacity here is 91.5 mAh/g after 10 cycles (Fig. 3b), further suggesting the good and reversible cycling performances in non-aqueous systems. As the currents increase, the polarization increases and the capacities decrease (Fig. 3c). While the initial discharge capacity of this nanocomposite at 5 C is 57.4 mAh/g, the discharge capacities at 10 C and 20 C are 25.0 and 9.9 mAh/g and much smaller than that at 1 C. At 1C, the discharge capacities remain quite stable after forty cycles (Fig. 3d).

pH has been proved to significantly affect the cycling performances of many electrode materials in aqueous LIBs and SIBs [23, 24]. Figure 4 shows CV curves of the nanocomposite in 1.0 M aqueous Na_2SO_4 solution at different pH in an oxygen-free environment in which the electrode hydrolysis was inhibited [23]. For the first scan at the initial pH = 4.0 (Fig. 4a), there is a pair of well-defined redox peaks: ∼0.465 V for the oxidation peak and ∼0.373 V for the reduction peak. From the second scan to the fifth scan, while both the oxidation currents at ∼0.465 V and reduction currents at ∼0.373 V decreased, the positions and shapes of these redox peaks remained the same. Meanwhile, shoulder peaks close to ∼0.373 V appeared in the reduction processes and the currents of those shoulder peaks only decreased very slightly possibly due to very slight dissolution of $Na_3V_2(PO_4)_3$ nanoparticles.

Currently, the mechanisms of the Na-ion extraction from $Na_3V_2(PO_4)_3$ during charge processes in non-aqueous systems are still being debated. Gu, Xi, and Hu suggested Na1 ions at the M1 (6b) sites tend to remain immobilized, only Na2 ions at the M2 (18e) sites could be extracted, and the Na-ion extraction process involve a two-phase transformation from $Na_3V_2(PO_4)_3$ to $NaV_2(PO_4)_3$ [12]. In contrast, Ji and Banks suggested that Na-ions at both sites could be extracted and the transformation from $Na_3V_2(PO_4)_3$ to $NaV_2(PO_4)_3$ involve $Na_2V_2(PO_4)_3$ as an intermediate [25]. From the second scan to the fifth scan in repeated CV scanning (Fig. 4a), should peaks near ∼0.373 V showed up and the oxidation peaks at ∼0.465 V are apparently broader than the reduction peaks at ∼0.373 V (Fig. 4a). All these observations suggest $Na_2V_2(PO_4)_3$ could serve as an intermediate in the two-step Na-ion insertion process but not the one-step Na-ion extraction process. Such difference indicates mechanisms or kinetics of Na-ion insertion and extractions differ, and similar phenomena in the metal-ion insertion and extraction in aqueous systems were observed before [26]. From the fifth scan to the tenth scan, the oxidation peaks shifted negatively slightly (∼0.457 V for the tenth scan) while the reduction peaks at ∼0.373 V shifted positively slightly (∼0.390 V for the tenth scan), suggesting possible structural reorganization.

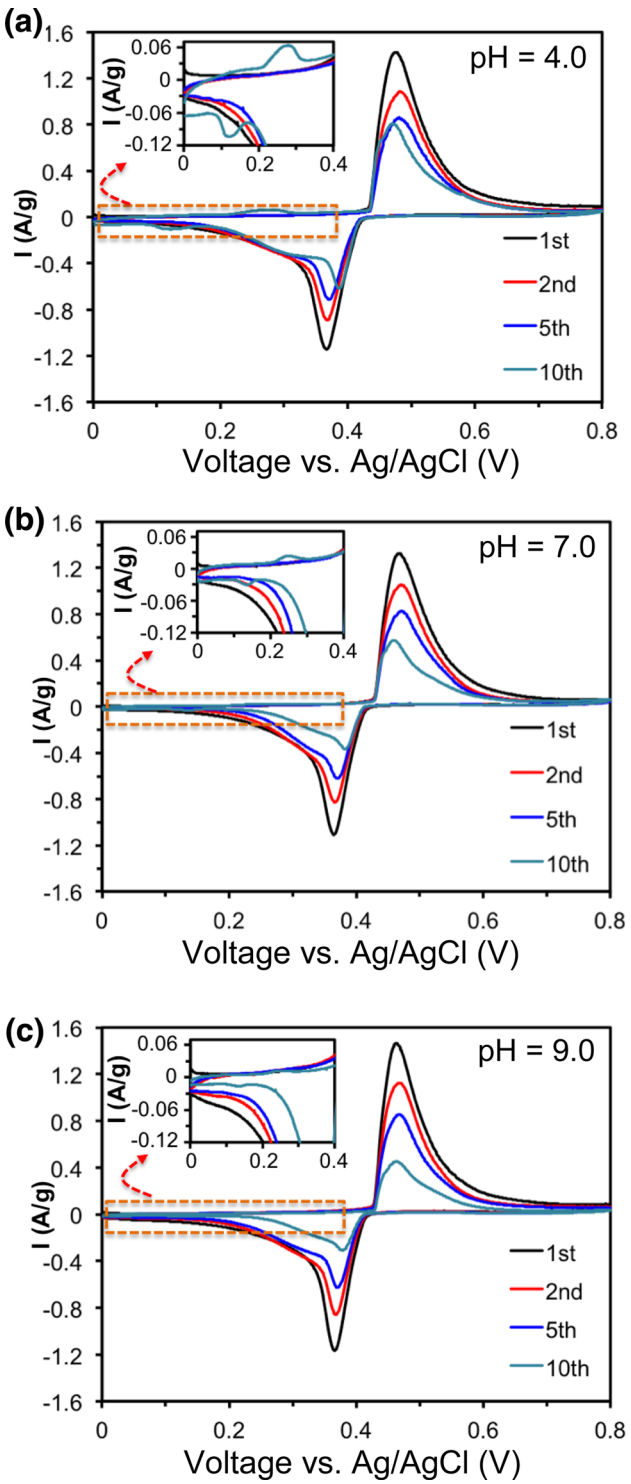

Fig. 4 Cyclic voltammograms (CVs) for $Na_3V_2(PO_4)_3$/C in 1 M aqueous Na2SO4 solution up to ten cycles at the scan rate of 0.5 mV/s at the initial pH = 4.0 (**a**), 7.0 (**b**), and 9.0 (**c**), respectively

After the fifth scan of CVs at pH = 4.0, an additional pair of weaker redox peaks (~0.270 and ~0.130 V) started to intensify (top left insets in Fig. 4a). These redox peaks are more prominent than those at pH = 7.0 and 9.0 (top left inset in Fig. 4b, c), suggesting such redox reactions could be related to the H^+ intercalation. Such H^+ intercalation in aqueous LIBs was observed to be irreversible [27]. Since $Na_3V_2(PO_4)_3$ has large interstitial spaces, $Na_3V_2(PO_4)_3$ may support reversible H^+ insertion-extraction. Such redox peaks were not reported before in both aqueous [10] and non-aqueous SIBs [7] using $Na_3V_2(PO_4)_3$ as cathode materials. The reason could be due to the later-described deterioration of crystallinity and structure that could favor the subsequent H^+ insertion-extraction. The corresponding redox currents being more than one order of magnitude lower than the major redox currents suggest low extent of H^+ insertion-extraction, which was confirmed by ICP analysis (the mole ratios of Na: P for electrodes before cycling and after five scans were found to be 1.00 and 0.98, respectively).

From the fifth scan to the tenth scan at pH = 4.0, the redox currents decreased in a much slower fashion than those at pH = 7.0 and 9.0 (Fig. 4a–c). The reason could be due to higher solubility of this nanocomposite's $Na_3V_2(PO_4)_3$ at higher pH, which was previously observed in the case of vanadium oxide [24].

It is worthy to note that during cycling the pH of electrolyte changed only slightly, especially for the cases of pH = 4.0 and 9.0. Equations (1) and (2) show the electrochemical processes during charge in both the working electrode and counter electrode:

$$Na_3V_2(PO_4)_3 \rightarrow NaV_2(PO_4)_3 + 2Na^+ + 2e^- \quad (1)$$

$$2H_2O + 2Na^+ + 2e^- \rightarrow 2NaOH + H_2 \quad (2)$$

Since the total mass of each electrode is only about 0.3 mg while the electrolyte is about 10 mL, the concentration of generated OH^- during charge is about 7.9×10^{-5} M. During the subsequent discharge, these OH^- are consumed. Therefore, the pH of the electrolyte with the initial pH being 4.0 is expected to range from 4.0 to 4.7 during cycling. The electrolytes with the initial pH being 7.0 and 9.0 are expected to be in the range of 7.0–9.9 and 9.0–9.95 respectively during cycling. Our experimental pH values matched these expected values. More in-depth investigations of the $Na_3V_2(PO_4)_3$-water interactions, its pH-dependent solubility, and optimization of electrolytes are beyond the scope of the paper and will be published separately.

On the basis of the above observations, pH = 4.0 was found to be an optimal condition for evaluating the cycling performances. pH lower than 4.0 was not employed since it could induce more H^+ intercalation and/or even hydrogen evolution. Figure 5a shows the charge–discharge profiles at a current of 1 C in the range of 0–0.8 V vs. Ag/AgCl. Upon assembly, the cell was charged to 0.8 V first and interestingly two close plateaus (~0.390 and ~0.430 V with the average being ~0.410 V) were observed for the first time possibly due to $Na_2V_2(PO_4)_3$ being as the intermediate during the charge (sodium extraction) process [25] or some kind(s) of structural reorganization. During the first discharge process, a major voltage plateau at ~0.405 V showed up. The low polarization (~0.005 V) is much smaller than 0.25 V observed in the non-aqueous electrolyte and indicates excellent ionic and electronic conductivities during this cycle. As the cycling continued, the charge–discharge profiles from the second to the tenth cycle demonstrated the following trends: (1) the polarization for the redox peaks at ~0.410 V kept increasing (0.029, 0.034, and 0.054 V for the second, fifth, and tenth cycles), suggesting continuously decreased ionic and electronic conductivities which could come from the deterioration of the $Na_3V_2(PO_4)_3$ nanoparticle's crystallinity and structure and/or the breakage of the carbon matrix; (2) an unobvious plateau showed up at ~0.200 V during discharge processes, and could attribute to the H^+-insertion processes; (3) the charge–discharge plateaus at ~0.410 V became narrower while the discharge plateaus at ~0.200 V became wider. Accordingly, the capacity fade around the voltage plateaus of ~0.410 V was somehow compensated by the capacity increase around those of ~0.200 V. In the tenth cycle, the voltage plateau around 0.410 V during the charge process was not strictly flat. All these trends match those observed during repeated CV scanning. As the currents increase, both the polarization increases and the capacity decreases (Fig. 5b) were less significant than those in the non-aqueous system due to faster kinetics in the aqueous system. The initial discharge capacities of this nanocomposite at 5 C, 10 C, and 20 C are 33.7, 18.3, and 11.6 mAh/g respectively. It is worthy to note the discharge capacity at 20 C in the aqueous system is even slightly higher than that in the non-aqueous system (9.9 mAh/g).

The charge and discharge capacities decrease relatively fast from the first cycle to the fifth cycle and then decrease much slower from the fifth cycle to the tenth cycle. Such trends match those of the redox currents at ~0.465 and ~0.373 V during repeated CV scanning. To understand such trends, ex situ PXRD analysis was used to analyze the pristine electrode and the electrode after five charge–discharge cycles at pH = 4.0 (Fig. 5c). All the major peaks remained, indicating the main framework remained after five cycles. However, the PXRD pattern of the electrode after cycling is indeed different from that of the pristine electrode in two aspects: First, the two pairs of split peaks in the PXRD pattern of the pristine electrode, namely

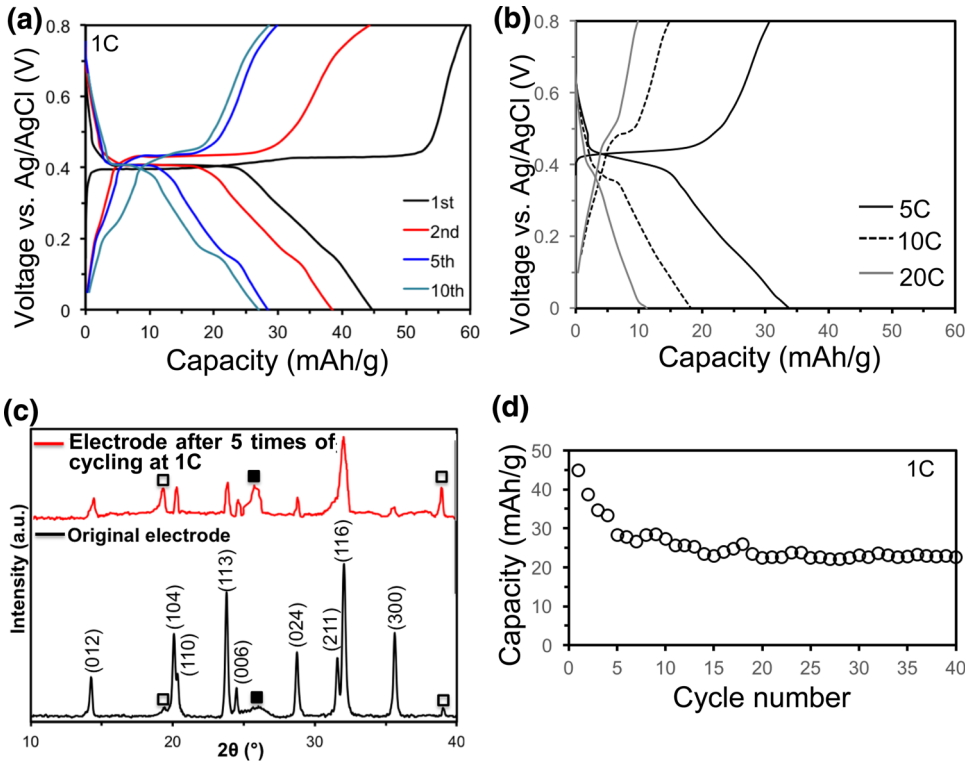

Fig. 5 **a** Galvanostatic charge–discharge cycling profiles of $Na_3V_2(PO_4)_3$/C nanocomposite in a 1 M Na_2SO_4 electrolyte at pH = 4.0 at 1 C. **b** Initial charge–discharge cycling profiles at pH = 4.0 at 5 C, 10 C, and 20 C. **c** PXRD patterns of electrodes before and after five cycles (*unfilled square* and *filled square* represent peaks from the stainless steel foil and super P carbon black, respectively); **d** Discharge capacity evolution for 40 cycles at 1 C currents

(104)/(110) and (211)/(116), were found to merge into two broad peaks, indicating the crystallinity of $Na_3V_2(PO_4)_3$ nanoparticles deteriorated during the cycling. Second, the intensity of the starting third-strong (300) peak relative to the strongest (116) peak was found to significantly decrease after the cycling. In contrast, such $Na_3V_2(PO_4)_3$ nanoparticles could maintain good crystallinity even after being cycled at 100 C for 1000 cycles in non-aqueous electrolytes [10]. Therefore, repeated Na-ion diffusion along the a axis should not be responsible for the deterioration of both crystallinity and structure of $Na_3V_2(PO_4)_3$ nanoparticles. Possible reasons could be the interactions between water molecules and $Na_3V_2(PO_4)_3$ nanoparticle including its crystallographic planes since both phosphates [28] and vanadium oxides [29] turned out to have interesting interfacial chemistry in aqueous systems.

Based on all these observations, we propose that the capacity fade during cycling should be mainly due to the deterioration of crystallinity and structure of the nanocomposite during the initial several charge–discharge cycles, some H^+ insertion-extraction, and slow dissolution of $Na_3V_2(PO_4)_3$ nanoparticles.

The discharge capacity of our $Na_3V_2(PO_4)_3$/C nanocomposite at 1 C rate in the first cycle in aqueous SIBs is 44.7 mAh/g. Considering the discharge capacities of both aqueous LIBs and SIBs are generally lower than those of their non-aqueous counterparts [23, 30], the capacity of this nanocomposite is quite decent. It is also close to that of previously reported $Na_3V_2(PO_4)_3$ microparticle discharged at 8.5 C in the first cycle (209 F/g, i.e. ~46.4 mAh/g), but the capacity retention rate of this nanocomposite (Fig. 5d) is much higher than that of the microparticle (50 vs. 31 % after thirty cycles) [16] though less than that observed in the non-aqueous system (Fig. 3c). It is worthy to note that the capacity fade is faster at current rates lower than 1C, possibly due to the slow dissolution of the electrode materials and/or the interactions between electrode materials and electrolytes during cycling [31].

Conclusions

In summary, compared to $Na_3V_2(PO_4)_3$ microparticle [16], this $Na_3V_2(PO_4)_3$/C nanocomposite demonstrated comparable discharge capacity during the first cycle in aqueous SIBs but much higher cycling stability in subsequent cycling. The carbon support capable of helping protect the electrode materials from aqueous electrolyte along with the optimal pH should be responsible for the significant improvement. The capacity fade should be mainly due to (1) the deterioration of both crystallinity and structure of the $Na_3V_2(PO_4)_3$ nanoparticle and (2) the possible breakage of the carbon matrix. The former should be due to the interactions between $Na_3V_2(PO_4)_3$ nanoparticle and electrolytes and could lead to the decreased ionic and electronic conductivities while the latter could lead to

decreased electronic conductivities. H^+ intercalation and slow dissolution of electrode materials are also partially responsible for the capacity fade.

Therefore, to further optimize the cycling stability of $Na_3V_2(PO_4)_3$ micro/nanoparticles in aqueous SIBs, the interactions between $Na_3V_2(PO_4)_3$ particles and water need to be minimized via either effective coating or wrapping of electrically conductive thin-layers onto particles. Ideally, these layers should meet the following criteria: (1) Flexible so that it could accommodate volume changes during cycling; (2) Water-proof but Na^+-conducting so that it could minimize the $Na_3V_2(PO_4)_3$-water interactions but facilitate the Na-ion diffusion. Carbon species such as graphene were proved to be a good Na-ion conductor and protecting reagent [1, 32]. Different types [22, 33] and amount [1] of carbon species were proved to significantly affect the cycling performances of NASCICON nanoparticles in both non-aqueous and aqueous SIBs. Optimization of such carbon coating/wrapping on $Na_3V_2(PO_4)_3$ nanoparticles for aqueous SIBs is ongoing.

Acknowledgments We appreciate Mr. Tyler Chism, Dr. Mourad Benamara, and Erik D. Pollock at the University of Arkansas for their help in materials synthesis, TEM and ICP-MS analysis. We also appreciate Mr. Seyed A. Ghetmiri and Dr. Shui-Qing Yu at the University of Arkansas for their assistance in Raman measurement. Dr. Jian-jun Zhang at Dalian University of Technology is also appreciated for his help in using PLATON to calculate the porosity of crystal structures.

References

1. Li, X.N., Zhu, X.B., Liang, J.W., Hou, Z.G., Wang, Y., Lin, N., Zhu, Y.C., Qian, Y.T.: Graphene-supported $NaTi_2(PO_4)_3$ as a high rate anode material for aqueous sodium ion batteries. J. Electrochem. Soc. **161**, A1181–A1187 (2014)
2. Li, Z., Young, D., Xiang, K., Carter, W.C., Chiang, Y.M.: Towards high power high energy aqueous sodium-ion batteries: The $NaTi_2(PO_4)_3/Na_{0.44}MnO_2$ system. Adv. Energy. Mater. **3**, 290–294 (2013)
3. Park, S.I., Gocheva, I., Okada, S., Yamaki, J.I.: Electrochemical properties of $NaTi_2(PO_4)_3$ anodes for rechargeable aqueous sodium-ion batteries. J. Electrochem. Soc. **158**, A1067–A1070 (2011)
4. Wu, W., Mohamed, A., Whitacre, J.F.: Microwave synthesized NaTi2(PO4)3 as an aqueous sodium-ion negative electrode. J. Electrochem. Soc. **160**(3), A497–A504 (2013)
5. Wu, X.Y., Sun, M.Y., Shen, Y.F., Qian, J.F., Cao, Y.L., Ai, X.P., Yang, H.X.: Energetic aqueous rechargeable sodium-ion battery based on $Na_2CuFe(CN)_6$-$NaTi_2(PO_4)_3$ intercalation chemistry. ChemSusChem. **7**(2), 407–411 (2014)
6. Qin, H., Song, Z.P., Zhan, H., Zhou, Y.H.: Aqueous rechargeable alkali-ion batteries with polyimide anode. J. Power Sources **249**, 367–372 (2014)
7. Kumar, P.R., Jung, Y.H., Lima, C.H., Kim, D.K.: $Na_3V_2O_{2x}(PO_4)_2F_{3-2x}$: a stable and high-voltage cathode material for aqueous sodium-ion batteries with high energy density. J. Mater. Chem. A **3**, 6271–6275 (2015)
8. Mason, C.W., Lange, F.: Aqueous ion battery systems using sodium vanadium phosphate stabilized by titanium substitution. ECS Electrochem. Lett. **4**(8), A79–A82 (2015)
9. Zatovsky, I.V.: NASICON-type $Na_3V_2(PO_4)_3$. Acta Cryst. **E66**, i12 (2010)
10. Zhu, C.B., Song, K.P., van Aken, P.A., Maier, J., Yu, Y.: Carbon-coated $Na_3V_2(PO_4)_3$ embedded in porous carbon matrix: an ultrafast Na-storage cathode with the potential of outperforming Li cathodes. Nano Lett. **14**, 2175–2180 (2014)
11. Jian, Z.L., Zhao, L., Pan, H.L., Hu, Y.S., Li, H., Chen, W., Chen, L.Q.: Carbon coated $Na_3V_2(PO_4)_3$ as novel electrode material for sodium ion batteries. Electrochem. Commun. **14**, 86–89 (2012)
12. Jian, Z.L., Yuan, C.C., Han, W.Z., Lu, X., Gu, L., Xi, X.K., Hu, Y.S., Li, H., Chen, W., Chen, D.F., Ikuhara, Y., Chen, L.Q.: Atomic structure and kinetics of NASICON $Na_xV_2(PO_4)_3$ cathode for sodium-ion batteries. Adv. Funct. Mater. **24**, 4265–4272 (2014)
13. Plashnitsa, L.S., Kobayashi, E., Noguchi, Y., Okada, S., Yamakia, J.I.: Performance of NASICON symmetric cell with ionic liquid electrolyte. J. Electrochem. Soc. **157**(4), A536–A543 (2010)
14. Aragon, M.J., Lavela, P., Ortiz, G.F., Tirado, J.L.: Effect of iron substitution in electrochem. Performance of Na3V2(PO4)3 as cathode for Na-ion batteries. J. Electrochem. Soc. **162**(2), A3077–A3083 (2015)
15. Jian, Z.L., Han, W.Z., Lu, X., Yang, H.X., Hu, Y.S., Zhou, J.: Superior electrochemical performance and storage mechanism of $Na_3V_2(PO_4)_3$ cathode for room-temperature sodium-ion batteries. Adv. Energy Mater. **3**, 156–160 (2013)
16. Song, W.X., Ji, X.B., Zhu, Y.R., Zhu, H.J., Li, F.Q., Chen, J., Lu, F., Yao, Y.P., Banks, C.E.: Aqueous sodium-ion battery using a $Na_3V_2(PO_4)_3$ electrode. ChemElectrochem **1**, 871–876 (2014)
17. Song, W.X., Ji, X.B., Wu, Z.P., Zhu, Y.R., Yang, Y.C., Chen, J., Jing, M.J., Li, F.Q., Banks, C.E.: First exploration of Na-ion migration pathways in the NASICON structure $Na_3V_2(PO_4)_3$. J. Mater. Chem. A **2**, 5358–5362 (2014)
18. Spek, A.L.: PLATON, Version 1.62, University of Utrecht, 1999
19. Shannon, R.D.: Revised effective ionic radii and systematic studies of interatomic distances in halides and chaleogenides. Acta Crystallogr. A **32**, 751–767 (1974)
20. Feng, Q., Miyai, Y., Kanoh, H., Ooi, L.: Hydrothermal synthesis of lithium and sodium manganese oxides and their metal ion extraction-insertion reactions. Chem. Mater. **7**, 1226–1232 (1995)
21. Kim, D.H., Kim, J.: Synthesis of LiFePO4 nanoparticles in polyol medium and their electrochemical properties. Electrochem. Solid-State Lett. **9**(9), A439–A442 (2006)
22. Li, S., Dong, Y.F., Xu, L., Xu, X., He, L., Mai, L.Q.: Effect of carbon matrix dimensions on the electrochemical properties of $Na_3V_2(PO_4)_3$ nanograins for high-performance symmetric sodium-ion batteries. Adv. Mater. **26**, 3545–3553 (2014)
23. Li, Z., Ravnsbæk, D.B., Xiang, K., Chiang, Y.M.: $Na_3Ti_2(PO_4)_3$ as a sodium-bearing anode for rechargeable aqueous sodium-ion batteries. Electrochem. Commun. **44**, 12–15 (2014)
24. Zhang, M.J., Dahn, J.R.: Electrochemical lithium intercalation in VO_2 (B) in aqueous electrolytes. J. Electrochem. Soc. **143**, 2730–2735 (1996)

25. Song, W.X., Cao, X.Y., Wu, Z.P., Chen, J., Huangfu, K.L., Wang, X.W., Huang, Y.L., Ji, X.B.: A study into the extracted ion number for NASICON structured $Na_3V_2(PO_4)_3$ in sodium-ion batteries. Phys. Chem. Chem. Phys. **16**, 17681–17687 (2014)
26. Kanoh, H., Tang, W.P., Makita, Y., Ooi, K.: Electrochemical intercalation of alkali-metal ions into birnessite-type manganese oxide in aqueous solution. Langmuir **13**, 6845–6849 (1997)
27. Wang, Y.G., Lou, J.Y., Wu, W., Wang, C.X., Xia, Y.Y.: Hybrid aqueous energy storage cells using activated carbon and lithium-ion intercalated compounds III. capacity fading mechanism of $LiCo_{1/3}Ni_{1/3}Mn_{1/3}O_2$ at different pH electrolyte solutions. J. Electrochem. Soc. **154**(3), A228–A234 (2007)
28. Bell, L.C., Posner, A.M., Quirk, J.P.: The point of zero charge of hydroxyapatite and fluorapatite in aqueous solutions. J. Colloid. Interf. Sci. **42**(2), 250–261 (1973)
29. Parks, G.A.: The isoelectric points of solid oxides, solid hydroxides, and aqueous hydroxo complex systems. Chem. Rev. **65**(2), 177–198 (1965)
30. Wang, G.J., Fu, L.J., Zhao, N.H., Yang, L.C., Wu, Y.P., Wu, H.Q.: An aqueous rechargeable lithium battery with good cycling performance. Angew. Chem. Int. Ed. **46**, 295–297 (2007)
31. Luo, J.Y., Cui, W.J., He, P., Xia, Y.Y.: Raising the cycling stability of aqueous lithium-ion batteries by eliminating oxygen in the electrolyte. Nat. Chem. **2**, 760–765 (2010)
32. Wei, D.H., Liang, J.W., Zhu, Y.C., Yuan, Z.Q., Li, N., Qian, Y.T.: formation of graphenewrapped nanocrystals at room temperature through the colloidal coagulation effect. Part. Part. Syst. Char. **30**, 143–147 (2013)
33. Zhao, B.D., Lin, B., Zhang, S., Deng, C.: A frogspawn-inspired hierarchical porous NaTi2(PO4)3-C array for high-rate and long-life aqueous rechargeable sodium batteries. Nanoscale **7**(44), 18552–18560 (2015)